DE G

Fractional Calculus & Applied Analysis
An International Journal for Theory and Applications
VOLUME 22, NUMBER 6 (2019)
(Print) ISSN 1311-0454
(Electronic) ISSN 1314-2224

RESEARCH PAPER

MASS-CONSERVING TEMPERED FRACTIONAL DIFFUSION IN A BOUNDED INTERVAL

Anna Lischke [1], **James F. Kelly** [2], **Mark M. Meerschaert** [3]

This paper is dedicated to the memory of late Professor Wen Chen

Abstract

Transient anomalous diffusion may be modeled by a tempered fractional diffusion equation. A reflecting boundary condition enforces mass conservation on a bounded interval. In this work, explicit and implicit Euler schemes for tempered fractional diffusion with discrete reflecting or absorbing boundary conditions are constructed. Discrete reflecting boundaries are formulated such that the Euler schemes conserve mass. Conditional stability of the explicit Euler methods and unconditional stability of the implicit Euler methods are established. Analytical steady-state solutions involving the Mittag-Leffler function are derived and shown to be consistent with late-time numerical solutions. Several numerical examples are presented to demonstrate the accuracy and usefulness of the proposed numerical schemes.

MSC 2010: Primary 26A33; Secondary 65M06, 33E12, 65N12

Key Words and Phrases: tempered fractional derivatives; discrete reflecting boundary conditions; finite difference methods; stability analysis

1. Introduction

The space-fractional diffusion equation with order $1 < \alpha < 2$ models anomalous super-diffusion, where a particle plume spreads faster than

pp. 1561–1595 , DOI: 10.1515/fca-2019-0081 DE GRUYTER

a plume modeled by the traditional diffusion equation. In the stochastic model underlying the space-fractional equation, the probability distribution of jump length follows a power law, hence some of its moments are undefined. Exponential tempering is used to cool these long jumps, and the resulting transient super-diffusion model is known as the tempered fractional diffusion (TFD) equation. The resulting plume exhibits super- and/or sub-diffusive spreading over some range of times, with a return to classical spreading for large times, which is referred to as *transient anomalous diffusion*.

Transient anomalous sub- and super-diffusion may be modeled with tempered time-fractional [30] and space-fractional [3] derivatives, respectively. Many applications in turbulence modeling [6, 13], astrophysics [5], economics [26], and plasma physics [19] exhibit power-law scaling over a range of space or time scales, with a return to Fickian diffusion at large distances or times, respectively. In sub-surface hydrology, complex geological media may contain both low-permeability deposits and preferential flow paths, which may be quantified by a combination of tempered space-fractional and time-fractional derivatives [42]. In river-flow hydrology, a quantitative comparison of various fractional calculus models applied to contaminant transport demonstrated that a tempered fractional model best captured the heavy-tailed breakthrough curves with a return to Fickian diffusion at late times [20]. A recent summary of quantum transport in one-dimensional mesoscopic systems showed that tempered fractional equations characterize media that is homogeneous at a large scale and fractal at an intermediate scale [35]. In all of these examples, the tempered fractional equation is formulated on the real line with no attention paid to the finite boundary.

Mass-conserving, reflecting boundary conditions for fractional PDEs (FPDEs) are needed to model anomalous diffusion in bounded domains. For example, super-diffusive dispersion in disordered porous media is observed in underground aquifers [4] and in rivers [7]. Reflecting boundary conditions have recently been used for both the forward [41] and backward [43] modeling of contaminant transport in aquifers and rivers. A recent series of papers [1, 2, 21] developed analytical and numerical methods for physically meaningful boundary conditions associated with space-fractional diffusion equations without tempering. These reflecting boundary conditions are based on a discrete representation of the fractional diffusion process in a bounded domain, where mass may impact the boundary from points far inside the domain. These boundary conditions were recently applied to surface hydrology in rivers using a fractional advection dispersion equation (FADE) [45].

Finite difference methods for space-tempered fractional diffusion models with Dirichlet (absorbing) boundary conditions have been studied in [9, 11, 23, 36]. In these articles, versions of tempered Grünwald-Letnikov finite difference schemes were presented for solving tempered fractional diffusion equations with Dirichlet boundary conditions. In [10], reflecting boundaries for tempered fractional diffusion operators were discussed in the context of demonstrating the well-posedness of PDEs with generalized boundary conditions. Unlike the boundary conditions proposed in [1] and [21], the reflecting conditions discussed in [10] are imposed at all points outside the domain, and hence differ qualitatively from the discrete boundary conditions proposed in the current paper. Although a reflecting boundary condition for tempered space-fractional equations was proposed in [45], a finite-difference scheme for this equation was not provided. To date, no numerical methods have been published that approximate the solution to tempered fractional diffusion models with mass-conserving reflecting boundary conditions.

In this work, explicit and implicit Euler methods for tempered space-fractional diffusion equations on a finite interval are developed with an emphasis on discrete reflecting boundary conditions. Conditional stability of the explicit schemes and unconditional stability of the implicit schemes for all combinations of reflecting and absorbing boundary conditions are proved, thereby extending the stability results of [3] to the tempered case. An analytical steady-state solution is derived and compared with numerical results using discrete reflecting boundary conditions. The highlight of this paper is discrete, mass-conserving boundary conditions for tempered space-fractional diffusion equations that are implemented within explicit and implicit finite-difference schemes.

Section 2 contains the notation and definitions of the fractional integrals and derivatives used in this work. In Section 3, consistent implicit and explicit Euler methods for tempered fractional diffusion equations are derived. Stability of the Euler schemes with reflecting or absorbing conditions is established in Section 4. Steady-state solutions for the tempered fractional diffusion equations with reflecting boundary conditions are discussed in Section 5. Section 6 contains numerical examples demonstrating the effect of the tempering parameter, the consistency of the numerical schemes with the steady-state solution, and convergence studies of the implicit and explicit Euler schemes.

2. **Tempered fractional diffusion equations**

Tempered fractional derivatives can be defined by modifying the classical Riemann-Liouville fractional derivative.

Definition 2.1. ([12]) On the real line, the positive Riemann-Liouville (RL) derivative of order $n-1 < \alpha < n$ with $n \in \mathbb{N}$ is defined

$$\mathbb{D}_+^\alpha f(x) = \frac{d^n}{dx^n}\mathbb{I}_+^{n-\alpha} f(x) = \frac{1}{\Gamma(n-\alpha)}\frac{d^n}{dx^n}\int_{-\infty}^{x}(x-y)^{n-\alpha-1} f(y)\,dy, \quad (2.1)$$

where $\mathbb{I}_+^{n-\alpha}$ is the positive Riemann-Liouville fractional integral. On a bounded interval $[L,R]$, the positive Riemann-Liouville derivative becomes

$$\mathbb{D}_{L^+}^\alpha f(x) = \frac{d^n}{dx^n}\mathbb{I}_{L^+}^{n-\alpha} f(x) = \frac{1}{\Gamma(n-\alpha)}\frac{d^n}{dx^n}\int_{L}^{x}(x-y)^{n-\alpha-1} f(y)\,dy, \quad (2.2)$$

with $L < x < R$.

The *tempered* Riemann-Liouville (TRL) fractional derivative is defined by multiplying the power-law convolution kernel of the Riemann-Liouville derivative (2.2) by a decaying exponential function.

Definition 2.2. Let $\lambda > 0$. Then the positive *tempered Riemann-Liouville derivative* of order $n-1 < \alpha < n$ with $n \in \mathbb{N}$ on the interval $[L,R]$ is defined by

$$\begin{aligned}\mathbb{D}_{L^+}^{\alpha,\lambda} f(x) &= e^{-\lambda x}\mathbb{D}_{L^+}^{\alpha}(e^{\lambda x} f(x)) \\ &= \frac{1}{\Gamma(n-\alpha)}\frac{d^n}{dx^n}\int_{L}^{x}\frac{e^{-\lambda(x-y)}}{(x-y)^{-n+\alpha+1}} f(y)\,dy.\end{aligned} \quad (2.3)$$

The TRL derivative on an unbounded domain $\mathbb{D}_+^{\alpha,\lambda} f(x)$ is recovered by setting the lower limit of integration in (2.3) to $-\infty$.

The tempered Riemann-Liouville derivative has been studied in [10, 36, 39, 40] as a tempered fractional diffusion operator.

The traditional fractional diffusion equation $\partial_t p(x,t) = C\mathbb{D}_+^\alpha p(x,t)$, $(x,t) \in \mathbb{R} \times [0,+\infty)$ with diffusion coefficient $C > 0$, order $1 < \alpha \leq 2$, and point-source initial condition $p(x,0) = \delta(x)$ has as its solution $p(x,t)$ that is the transition density of a positively skewed α-stable Lévy motion for which all moments of order two or larger are infinite [16]. To address the issue of infinite moments, one can *temper* the process by multiplying its density $p(x,t)$ by a decaying exponential, i.e., $e^{-\lambda x}p(x,t)$, where $\lambda > 0$ is the tempering parameter that is chosen according to the application. The function $f(x,t) = e^{-\lambda x}p(x,t)$ solves the *tempered* fractional differential equation

$$\partial_t f(x,t) = C\mathbb{D}_+^{\alpha,\lambda} f(x,t) \quad (x,t) \in \mathbb{R} \times [0,+\infty), \quad (2.4)$$

subject to $f(x,0) = \delta(x)$. This tempered fractional differential equation has been extensively studied in the literature [10, 23, 24, 36, 38, 39, 40].

REMARK 2.1. The spatial Fourier transform (FT) $\hat{f}(k) = \mathcal{F}[f(x)] = \int_{-\infty}^{\infty} f(x)e^{-ikx}\,dx$ of the TRL on an unbounded domain is computed using the shift property of Fourier transforms and the well-known FT of the RL derivative $\mathcal{F}\left[\mathbb{D}_{+}^{\alpha} f(x)\right] = (ik)^{\alpha}\hat{f}(k)$, yielding $\mathcal{F}\left[\mathbb{D}_{+}^{\alpha,\lambda} f(x)\right] = (\lambda + ik)^{\alpha}$ [27, Section 7.4]. Also see Eq. (2.5) in [23].

Applying a spatial FT to (2.4) and invoking this property yields $\partial_t \hat{f}(k,t) = C\left(\lambda + ik\right)^{\alpha}\hat{f}(k,t)$, which has solution

$$\hat{f}(k,t) = e^{Ct[(\lambda+ik)^{\alpha}]}, \tag{2.5}$$

assuming an impulse initial condition.

REMARK 2.2. The model (2.4) does not conserve mass. To see this, denote the total mass at time t by $M(t) = \int_{-\infty}^{\infty} f(x,t)\,dx$. The total mass $M(t)$ may be computed by setting $k = 0$ in (2.5), i.e., $M(t) = e^{C\lambda^{\alpha}t}$. Since M is not constant, mass is not conserved. This model cannot accurately be called a *diffusion* equation, since mass is added to the system over time.

In the remainder of this work, we focus on mass-preserving models of tempered fractional diffusion.

2.1. **Normalized tempered fractional diffusion.** In order to construct a mass-preserving model, the tempered pdf $e^{-\lambda x}p(x,t)$ must be normalized. Using the Fourier transform of f as written in Remark 2.2, the normalized tempered pdf is defined as the function $p_\lambda(x,t)$ with Fourier transform $\hat{p}_\lambda(k,t) = e^{Ct[(\lambda+ik)^{\alpha}-\lambda^{\alpha}]}$. This expression was achieved by normalizing by $M(t)$ in order for $p_\lambda(x,t)$ to have unit mass. Taking the time derivative of $\hat{p}_\lambda(k,t)$ yields

$$\partial_t \hat{p}_\lambda(k,t) = C[(\lambda + ik)^{\alpha} - \lambda^{\alpha}]\hat{p}_\lambda(k,t), \tag{2.6}$$

and applying the inverse Fourier transform to both sides of (2.6) yields the *normalized* tempered fractional diffusion equation

$$\partial_t p_\lambda(x,t) = C(\mathbb{D}_{+}^{\alpha,\lambda} p_\lambda(x,t) - \lambda^{\alpha} p_\lambda(x,t)). \tag{2.7}$$

The point-source solution of (2.7) subject to $p_\lambda(x,0) = \delta(x)$ is given by

$$p_\lambda(x,t) = e^{-Ct\lambda^{\alpha}} e^{-\lambda x} f_\alpha(x, Ct), \tag{2.8}$$

where $f_\alpha(x,t)$ is a positively-skewed α-stable density [46] given by the inverse FT

$$f_\alpha(x,t) = \frac{1}{2\pi}\int_{-\infty}^{\infty} e^{t(ik)^{\alpha}} e^{ikx}\,dk. \tag{2.9}$$

Definition 2.3. We refer to the operator $\mathbb{D}_+^{\alpha,\lambda} p_\lambda(x,t) - \lambda^\alpha p_\lambda(x,t)$ with $1 < \alpha \leq 2$ as the *normalized tempered Riemann-Liouville* (NTRL) *derivative*.

2.2. **Centered normalized tempered RL derivative.** Recall that the Fourier transform of $p_\lambda(x,t)$ is $e^{Ct[(\lambda+ik)^\alpha - \lambda^\alpha]}$ and note that the transition density $p_\lambda(x,t)$ is infinitely differentiable since the positively-skewed stable density $f_\alpha(x,t)$ is also infinitely differentiable [46]. Then the mean is computed as

$$\int_{-\infty}^{\infty} x p_\lambda(x,t)\,dx = \int_{-\infty}^{\infty} i\frac{d}{dk}(e^{-ikx})\Big|_{k=0} p_\lambda(x,t)\,dx = i\frac{d}{dk} e^{Ct[(\lambda+ik)^\alpha - \lambda^\alpha]}\Big|_{k=0} = -Ct\alpha\lambda^{\alpha-1}.$$

To center the density on the real line, the centered normalized tempered stable density $p_{\lambda,0}(x,t)$ is defined as the function with the Fourier transform

$$\hat{p}_{\lambda,0}(k,t) = e^{Ct[(\lambda+ik)^\alpha - \lambda^\alpha - ik\alpha\lambda^{\alpha-1}]}, \tag{2.10}$$

so that the mean of $p_{\lambda,0}(x,t)$ is zero. As before, taking the time derivative followed by the inverse Fourier transform of each side of (2.10) yields

$$\partial_t p_{\lambda,0}(x,t) = C\left(\mathbb{D}_+^{\alpha,\lambda} p_{\lambda,0}(x,t) - \lambda^\alpha p_{\lambda,0}(x,t) - \alpha\lambda^{\alpha-1}\partial_x p_{\lambda,0}(x,t)\right). \tag{2.11}$$

The point-source solution of (2.11) is given by

$$p_\lambda(x,t) = e^{Ct(\alpha-1)\lambda^\alpha} e^{-\lambda x} f_\alpha(x - Ct\alpha\lambda^{\alpha-1}, Ct). \tag{2.12}$$

Definition 2.4. We refer to the tempered fractional diffusion operator $\mathbb{D}_+^{\alpha,\lambda} p_{\lambda,0}(x,t) - \lambda^\alpha p_{\lambda,0}(x,t) - \alpha\lambda^{\alpha-1}\partial_x p_{\lambda,0}(x,t)$ with $1 < \alpha \leq 2$ as the *centered normalized tempered Riemann-Liouville* (CNTRL) *derivative*.

3. Euler methods for tempered fractional diffusion

In this section, explicit and implicit Euler methods are developed for tempered fractional diffusion equations (2.7) and (2.11) with reflecting boundary conditions. Our approach, which extends that of Baeumer et al. [1], requires that mass leaving the domain should instead come to rest at the boundary (an inelastic collision), which is enforced in the discretization. Particles undergoing tempered fractional diffusion may reach the boundary of the domain from interior nodes far from the boundary, resulting in a nonlocal flux.

3.1. **Grünwald-Letnikov approximations.** The Riemann-Liouville fractional derivative (2.1) of order $1 < \alpha \leq 2$ can be approximated according to the shifted Grünwald-Letnikov (GL) formula (see [29, Remark 2.2] and [27, Proposition 2.1])

$$\mathbb{D}_+^\alpha u(x,t) = h^{-\alpha} \sum_{i=0}^{\infty} g_i^\alpha u(x-(i-1)h,t) + \mathcal{O}(h), \tag{3.1}$$

where the shift is necessary for stability [28]. The Grünwald weights are defined

$$g_i^\alpha = (-1)^i \binom{\alpha}{i} = \frac{(-1)^i \Gamma(\alpha+1)}{\Gamma(i+1)\Gamma(\alpha-i+1)}.$$

These weights have the following properties for $1 < \alpha \leq 2$ [1]: (i) $g_i^\alpha > 0$ for all $i \neq 1$, (ii) $g_1^\alpha = -\alpha < 0$, and (iii) $\sum_{i=0}^{\infty} g_i^\alpha = 0$.

To approximate the NTRL derivative (2.3) on the real line $\mathbb{R}$, the GL formula is [3]

$$\begin{aligned} \mathbb{D}_+^{\alpha,\lambda} u(x,t) - \lambda^\alpha u(x,t) = h^{-\alpha} \sum_{i=0}^{\infty} g_i^\alpha e^{-\lambda h(i-1)} u(x-(i-1)h,t) \\ -h^{-\alpha} e^{\lambda h} \left(1 - e^{-\lambda h}\right)^\alpha u(x,t) + \mathcal{O}(h). \end{aligned} \tag{3.2}$$

As $h \to 0$, the term $h^{-\alpha} e^{\lambda h} (1 - e^{-\lambda h})^\alpha$ converges to λ^α so that this approximation converges to the NTRL derivative (2.3) [3]. Extending this approximation to the centered normalized tempered RL derivative is straightforward by approximating the first derivative term with a first-order finite difference.

3.2. **Normalized tempered fractional diffusion equation.** We develop explicit and implicit Euler schemes for the normalized TFD equation (2.7) on the bounded domain $[L, R]$ with mass-conserving (reflecting) and absorbing (zero Dirichlet) boundary conditions. Stable Crank-Nicolson [3] and higher-order schemes [23] for tempered fractional equations have previously been developed, but only for the case of absorbing boundary conditions.

First, the interval $[L, R]$ is discretized into $n+1$ points as $L = x_0 < x_1 < \cdots < x_n = R$, where the grid spacing is $h = x_i - x_{i-1} = (R-L)/n$. Similarly, the interval $[0, T]$ is discretized into $m+1$ points as $0 = t_1 < t_2 < \cdots < t_m = T$, where the time step is $\Delta t = t_k - t_{k-1} = T/m$. Let $u_i^k = u(x_i, t_k)$. The explicit Euler scheme is written

$$\frac{u_j^{k+1} - u_j^k}{\Delta t} = C h^{-\alpha} \sum_{i=0}^{j+1} b_{ij} u_i^k, \tag{3.3}$$

where the coefficients b_{ij} are proportional to mass moving from position x_i to position x_j, and are determined as follows.

The mass at position x_i and time t_k is given by hu_i^k, and the scheme (3.3) can be interpreted physically as follows. Let $\beta = Ch^{-\alpha}\Delta t$. When $i \neq j$, mass $\beta b_{ij} hu_i^k$ moves from x_i to x_j between times t_k and t_{k+1}. When x_i and x_j reside in the interior of $[L, R]$, the coefficient $b_{ij} = g_{j-i+1}^{\alpha} e^{-\lambda h(j-i)}$, which is determined using (3.1) (after a change of index). When $i = j$ and x_i again resides in the interior of the domain, the total mass leaving x_i is given by $\beta b_{ii} hu_i^k$, where $b_{ii} = g_1^{\alpha} - e^{\lambda h}(1 - e^{-\lambda h})^{\alpha} = -\alpha - e^{\lambda h}(1 - e^{-\lambda h})^{\alpha}$. In a mass-preserving scheme, the mass $-\beta b_{ii} hu_i^k$ leaving x_i must be equal to the mass $\beta \sum_{j=0, j\neq i}^{n} b_{ij} hu_i^k$ arriving at x_i.

When either x_i or x_j are on the boundaries of the interval $[L, R]$, b_{ij} is determined by modifying the GL coefficients such that mass cannot leave the domain. To do so, first consider the left boundary $x_0 = L$. Since the positive fractional derivative models mass that can take long jumps to the right and only short (h-sized) movements to the left, the only way mass can exit the boundary at the left endpoint is by moving from position x_0 to $x_{-1} = -h$. To keep this mass in the interval, we require that mass $\beta g_0^k e^{\lambda h} hu_0^k$ remains at x_0. Furthermore, the Grünwald approximation (3.2) requires that mass $\beta(e^{\lambda h}(1 - e^{-\lambda h})^{\alpha} - g_1^{\alpha}) hu_0^k$ exits position x_0 and jumps elsewhere in the domain within a given time step. Therefore,

$$b_{00} = g_1^{\alpha} - e^{\lambda h}(1 - e^{-\lambda h})^{\alpha} + g_0 e^{\lambda h}.$$

Next, consider the right boundary $x_n = R$. Mass that would jump from any position x_i inside the domain to positions $x_{n+1}, x_{n+2}, \ldots$, is reflected to stay in the domain via an inelastic collision with the right boundary $x_n = R$. In our reflecting scheme, the mass moving from position x_i for $i = 0, 1, \ldots, n-1$ to x_n is then

$$\beta \sum_{\ell=n}^{\infty} g_{\ell-i+1}^{\alpha} e^{-\lambda h(\ell-i)} u_i^k = \beta \sum_{\ell=n-i+1}^{\infty} g_{\ell}^{\alpha} e^{-\lambda h(\ell-1)} u_i^k. \tag{3.4}$$

To compute the infinite sum in (3.4), the binomial theorem $(x+y)^r = \sum_{k=0}^{\infty} \binom{r}{k} x^{r-k} y^k$ with $|x| > |y|$ is used. Then $\sum_{i=0}^{\infty} g_i^{\alpha} e^{-\lambda h(i-1)} = e^{\lambda h}(1 - e^{-\lambda h})^{\alpha}$, yielding

$$\beta \sum_{\ell=n-i+1}^{\infty} g_{\ell}^{\alpha} e^{-\lambda h(\ell-1)} u_i^k = \beta \left(e^{\lambda h}(1 - e^{-\lambda h})^{\alpha} - \sum_{\ell=0}^{n-i} g_{\ell}^{\alpha} e^{-\lambda h(\ell-1)} u_i^k \right). \tag{3.5}$$

Therefore, for $i = 0, 1, \ldots, n-1$,

$$b_{in} = e^{\lambda h}(1 - e^{-\lambda h})^{\alpha} - \sum_{\ell=0}^{n-i} g_{\ell}^{\alpha} e^{-\lambda h(\ell-1)}.$$

Finally, mass is only allowed to move out of position x_n by jumping to x_{n-1}, so

$$b_{nn} = -g_0^{\alpha} e^{\lambda h}.$$

The resulting matrix B with coefficients b_{ij} is defined by

$$b_{ij} = \begin{cases} g_{j-i+1}^{\alpha} e^{-\lambda h(j-i)} & 0 < i \le j+1, \ \ i \ne j, j+1, \\ & 0 < j < n-1, \\ g_1^{\alpha} - e^{\lambda h}(1 - e^{-\lambda h})^{\alpha} & 0 < i = j < n, \\ g_1^{\alpha} - e^{\lambda h}(1 - e^{-\lambda h})^{\alpha} + g_0^{\alpha} e^{\lambda h} & i = j = 0, \\ e^{\lambda h}(1 - e^{-\lambda h})^{\alpha} - \sum_{\ell=0}^{n-i} g_{\ell}^{\alpha} e^{-\lambda h(\ell-1)} & 0 \le i \le n-1, \ j = n, \\ -g_0^{\alpha} e^{\lambda h} & i = j = n, \\ 0 & i > j+1. \end{cases} \tag{3.6}$$

The implicit Euler scheme is written as

$$\frac{u_j^{k+1} - u_j^k}{\Delta t} = Ch^{-\alpha} \sum_{i=0}^{j+1} b_{ij} u_i^{k+1}, \tag{3.7}$$

where the coefficients $\{b_{ij}\}$ are defined as in (3.6).

PROPOSITION 3.1. *The diagonal entries of B in* (3.6) *are all negative, and the off-diagonal entries are non-negative.*

P r o o f. The diagonal entries b_{ii} where $i \ne 0$ and $i \ne n$ are given by $b_{ii} = g_1^{\alpha} - e^{\lambda h}(1 - e^{-\lambda h})^{\alpha}$. The coefficient $g_1^{\alpha} = -\alpha < -1$, which implies $b_{ii} < 0$ because $e^{\lambda h}(1 - e^{-\lambda h})^{\alpha} > 0$. When $i = 0$, $b_{00} = -\alpha - e^{\lambda h}(1 - e^{-\lambda h})^{\alpha} + g_0^{\alpha} e^{\lambda h}$. Note that $g_0^{\alpha} = 1$. Since

$$\sum_{i=0, i\ne 1}^{\infty} g_i^{\alpha} e^{-\lambda h(i-1)} = e^{\lambda h}(1 - e^{-\lambda h})^{\alpha} + \alpha,$$

and all terms in the sum are positive, $g_0^{\alpha} e^{\lambda h} < e^{\lambda h}(1 - e^{-\lambda h})^{\alpha} + \alpha$, which implies $b_{00} < 0$. If $i = n$, $b_{nn} = -g_0^{\alpha} e^{\lambda h} = -e^{\lambda h} < 0$. Therefore, all diagonal entries of B are negative.

Using the fact $g_i^{\alpha} > 0$ for all $i \ne 1$ and $e^{-\lambda hk} > 0$ for any integer k, $b_{ij} = g_{j-i+1}^{\alpha} e^{-\lambda h(j-i)} > 0$ for all $0 < i \le j+1$, $i \ne j, j+1$, and $0 < j < n-1$. If $0 \le i \le n-1$ and $j = n$, then we have $b_{ij} = e^{\lambda h}(1 -$

$e^{-\lambda h})^\alpha - \sum_{\ell=0}^{n-i} g_\ell^\alpha e^{-\lambda h(\ell-1)}$. Since $\sum_{\ell=0}^{\infty} g_\ell^\alpha e^{-\lambda h(\ell-1)} = e^{\lambda h}(1-e^{-\lambda h})^\alpha$, it follows that

$$b_{ij} = e^{\lambda h}(1-e^{-\lambda h})^\alpha - \sum_{\ell=0}^{n-i} g_\ell^\alpha e^{-\lambda h(\ell-1)} = \sum_{\ell=0}^{\infty} g_\ell^\alpha e^{-\lambda h(\ell-1)} - \sum_{\ell=0}^{n-i} g_\ell^\alpha e^{-\lambda h(\ell-1)}$$
$$= \sum_{\ell=n-i+1}^{\infty} g_\ell^\alpha e^{-\lambda h(\ell-1)}.$$

Since $i \le n-1$, we have $n-i+1 \ge 2$, so all terms of the final sum above are positive, and $b_{ij} > 0$. Recalling that $b_{ij} = 0$ for all $i > j+1$, it follows that all off-diagonal entries of B are non-negative. □

Remark 3.1. To implement absorbing boundary conditions applied to Equation (2.7), the modified coefficient matrix is given by (3.6) with all entries in rows $i = 0$ and $i = n$ set to zero. To implement an absorbing condition at the left boundary and a reflecting condition at the right boundary, the coefficient matrix is given by (3.6) with all entries in row $i = 0$ set to zero. Similarly, for an absorbing boundary condition on the right and a reflecting condition on the left, the coefficient matrix (3.6) should have all entries in row $i = n$ set to zero.

Proposition 3.2. *The explicit Euler scheme* (3.3) *and implicit Euler scheme* (3.7) *with B defined in* (3.6) *is mass-preserving, as for any fixed $i = 0, 1, \ldots, n$, we have $\sum_{j=0}^{n} b_{ij} = 0$.*

P r o o f. It is straightforward to verify that $\sum_{j=0}^{n} b_{ij} = 0$ for any i by writing out the sum for each i using the entries b_{ij} defined in (3.6). Hence the scheme redistributes the mass at each state x_i at each time step without changing the total mass. □

Remark 3.2. Although we focus on the case $1 < \alpha \le 2$ in this work, one can also consider the equation

$$\partial_t u(x,t) = -C(\mathbb{D}_+^{\alpha,\lambda} u(x,t) - \lambda^\alpha u(x,t))$$

with $0 < \alpha < 1$. In this case, the shift in the Grünwald formula (3.1) becomes unnecessary for stability. This model also conserves mass, and mass-preserving boundaries may also be enforced using a similar approach to the one described above.

3.3. **Centered normalized tempered fractional diffusion equation.** We also develop Euler schemes for the centered normalized TFD equation

(2.11) on the domain $(x,t) \in [L,R] \times [0,T]$ with combinations of reflecting and absorbing boundary conditions, as in Section 3.2. The stability results for these methods are proved in Section 4.1, and numerical examples are included in Section 6.

We determine the coefficients b_{ij}^0 using the same logic as above, where we $\partial_x u(x_j,t_k)$ is approximated via a backward difference. Letting $S_k = \sum_{\ell=0}^{k} g_\ell^\alpha e^{-\lambda h(\ell-1)}$ yields

$$b_{ij}^0 = \begin{cases} g_{j-i+1}^\alpha e^{-\lambda h(j-i)} & 0 < j < n,\ 0 \le i \le j+1, \\ & i \ne j-1, j, \\ g_1^\alpha - e^{\lambda h}(1-e^{-\lambda h})^\alpha - \alpha(\lambda h)^{\alpha-1} & 0 < i = j < n, \\ g_2^\alpha e^{-\lambda h} + \alpha(\lambda h)^{\alpha-1} & 0 \le i = j-1 \le n-2, \\ g_1^\alpha - e^{\lambda h}\left((1-e^{-\lambda h})^\alpha - g_0^\alpha\right) - \alpha(\lambda h)^{\alpha-1} & i = j = 0, \\ e^{\lambda h}(1-e^{-\lambda h})^\alpha - S_{n-i} & 0 \le i < n-1,\ \ j = n, \\ e^{\lambda h}(1-e^{-\lambda h})^\alpha - S_1 + \alpha(\lambda h)^{\alpha-1} & i = n-1,\ \ j = n, \\ -g_0^\alpha e^{\lambda h} & i = j = n, \\ 0 & i > j+1. \end{cases} \tag{3.8}$$

The resulting scheme is mass-preserving, which can be shown in the same way as in Proposition 3.2, since $\sum_{j=0}^{n} b_{ij}^0 = 0$ for any fixed $i = 0, 1, \ldots, n$. Incorporating absorbing boundary conditions for (2.11) can be achieved by modifying B^0 defined in (3.8) as described in Remark 3.1.

The explicit and implicit Euler schemes for both the normalized and centered models may be written compactly by defining a row vector with entries representing the solution at time t_k by $\boldsymbol{u}_k = [u(x_i,t_k)]$, so that $\boldsymbol{u}_{k+1} = \boldsymbol{u}_k + \beta \boldsymbol{u}_k B$. Then the explicit Euler scheme may be written

$$\boldsymbol{u}_{k+1} = \boldsymbol{u}_k A, \tag{3.9}$$

where $A = I + \beta B$. The implicit Euler scheme can be written as

$$\boldsymbol{u}_{k+1} M = \boldsymbol{u}_k, \tag{3.10}$$

where $M = I - \beta B$. The explicit and implicit schemes for the centered normalized model replaces B with B^0.

3.4. **Reflecting boundary conditions and flux functions.** In the case where $\lambda = 0$, reflecting boundary conditions for the fractional diffusion equation $\partial_t u(x,t) = \mathbb{D}_{L^+}^\alpha u(x,t)$ were derived by Baeumer et al. [1]. Defining the flux function $F(x,t) = \mathbb{D}_{L^+}^{\alpha-1} u(x,t)$, the non-tempered fractional diffusion equation may be written in conservation form as

$$\partial_t u(x,t) = -\partial_x F(x,t), \quad (x,t) \in [L,R] \times [0,\infty), \tag{3.11}$$

with the reflecting boundary conditions $F(L,t) = F(R,t) = 0$ written explicitly as

$$\mathbb{D}_{L^+}^{\alpha-1} u(x,t)\Big|_{x=L} = \mathbb{D}_{L^+}^{\alpha-1} u(x,t)\Big|_{x=R} = 0.$$

In the tempered case, it is difficult to write the flux analytically, since the α-tempered fractional derivative is not the first derivative of the $(\alpha-1)$-tempered fractional derivative. Hence, in the tempered case, it is not straightforward to write the reflecting boundary conditions in a simple analytical form.

4. Stability analysis

4.1. **Explicit Euler schemes.** In this section, we prove stability of the explicit Euler scheme for the normalized TFD equation with different combinations of absorbing and reflecting boundary conditions.

THEOREM 4.1. *Given the matrix B defined in* (3.6) *representing the discretized form of the normalized TFD equation* (2.7) *with reflecting boundary conditions, let A represent the iteration matrix of the explicit Euler scheme, i.e., $A = I + \beta B$ and $\beta = \Delta t C h^{-\alpha}$. If $\beta \le 1/\alpha$, then the explicit Euler method* (3.3) *is stable.*

Furthermore, if the matrix B is modified according to Remark 3.1 to incorporate absorbing boundary conditions at either the left, right, or both endpoints, and $\beta \le 1/\alpha$, the resulting explicit Euler scheme is also stable.

P r o o f. In order to show stability, we use the Gerschgorin circle theorem [18, pp. 135–136], so that the eigenvalues $\{\sigma_i^A\}$ of A satisfy $a_{ii} - r_i \le \sigma_i^A \le a_{ii} + r_i$, where

$$r_i = \sum_{j=0, j\neq i}^{n} |a_{ij}|.$$

The explicit Euler scheme is stable if

$$-1 \le a_{ii} - r_i \le \sigma_i^A \le a_{ii} + r_i \le 1. \tag{4.1}$$

Since the off-diagonal terms of B are non-negative, and $\sum_{j=0}^{n} b_{ij} = 0$,

$$r_i = \sum_{j=0, j\neq i}^{n} |a_{ij}| = \sum_{j=0, j\neq i}^{n} \beta b_{ij} = \sum_{j=0}^{n} \beta b_{ij} - \beta b_{ii} = -\beta b_{ii}.$$

Therefore, $\sigma_i^A \le a_{ii} - \beta b_{ii} = 1 + \beta b_{ii} - \beta b_{ii} = 1$. Next, consider the lower bound: $\sigma_i^A \ge a_{ii} + \beta b_{ii} = 1 + 2\beta b_{ii}$. In order for $\sigma_i \ge -1$, we will show that $1 + 2\beta b_{ii} \ge -1$, which holds when $\beta \le -1/b_{ii}$. We check the three cases: (i) $i = 0$, (ii) $0 < i < n$, and (iii) $i = n$.

Case 1. First, for $i = 0$, $b_{00} = g_1^\alpha - e^{\lambda h}(1 - e^{-\lambda h})^\alpha + g_0^\alpha e^{\lambda h} = -\alpha - e^{\lambda h}(1 - e^{-\lambda h})^\alpha + e^{\lambda h}$, which requires

$$\beta \leq \frac{1}{\alpha + e^{\lambda h}(1 - e^{-\lambda h})^\alpha - e^{\lambda h}}. \tag{4.2}$$

Case 2. Next, for $0 < i < n$, $b_{ii} = g_1^\alpha - e^{\lambda h}(1 - e^{-\lambda h})^\alpha = -\alpha - e^{\lambda h}(1 - e^{-\lambda h})^\alpha$, thus we require

$$\beta \leq \frac{1}{\alpha + e^{\lambda h}(1 - e^{-\lambda h})^\alpha}. \tag{4.3}$$

Case 3. Finally, for $i = n$, $b_{nn} = -e^{\lambda h}$, which means we must have

$$\beta \leq e^{-\lambda h}. \tag{4.4}$$

By inspection, the minimum of the right hand sides of (4.2), (4.3), and (4.4) is (4.3), where

$$\beta \leq \frac{1}{\alpha + e^{\lambda h}(1 - e^{-\lambda h})^\alpha} \leq \frac{1}{\alpha},$$

so that the stability condition is

$$\Delta t \leq \frac{h^\alpha}{\alpha C}. \tag{4.5}$$

This condition is the same as the stability condition for the scheme presented in [1]. So if (4.5) is satisfied, we have that $a_{ii} - r_i = 1 + 2\beta b_{ii} \geq -1$. Therefore, (4.1) is satisfied, and the reflecting explicit Euler scheme is stable according to the Gerschgorin circle theorem.

Suppose that B is modified to incorporate an absorbing boundary condition at the left endpoint according to Remark 3.1, so that $b_{0j} = 0$ for all j. Then $r_0 = \sum_{j=1}^n |a_{0j}| = 0$ and $a_{00} = 1$, which yields $a_{00} - r_0 = a_{00} + r_0 = 1$. Then the Gerschgorin circle theorem implies that $\sigma_0^A = 1$, with all the other eigenvalues also satisfying condition (4.1) as before, so the explicit Euler scheme is stable. This argument follows in the same way when an absorbing boundary condition is imposed on the right endpoint, so that $b_{nj} = 0$ for all j. Therefore, the explicit Euler schemes implementing any combination of absorbing and reflecting boundary conditions are all conditionally stable. □

REMARK 4.1. Stability of the explicit Euler scheme for centered normalized TFD equation for $\beta \leq 1/\alpha$ follows in exactly the same manner, except that the stability condition includes a contribution from the first derivative term, i.e.,

$$\beta \leq \frac{1}{\alpha + e^{\lambda h}(1 - e^{-\lambda h})^\alpha + \alpha(\lambda h)^{\alpha - 1}}.$$

This expression is bounded above by $1/\alpha$, yielding the stability condition (4.5).

4.2. **Stability of implicit Euler schemes.**

THEOREM 4.2. *Given the matrix B representing the discretized form of the normalized tempered diffusion operator with reflecting boundary conditions, let M represent the iteration matrix of the implicit Euler scheme, i.e., $M = I - \beta B$. The eigenvalues $\{\sigma^M\}$ of the matrix M satisfy $\sigma^M \geq 1$; hence, the implicit Euler method* (3.10) *is unconditionally stable.*

Furthermore, if the implicit Euler scheme is modified to incorporate absorbing boundary conditions at the left, right, or both endpoints by setting the appropriate rows of the matrix B to zero as described in Remark 3.1, the resulting scheme is again unconditionally stable.

P r o o f. Recall that the Gerschgorin circle theorem implies that, for each i, the eigenvalues σ_i^M of the matrix M satisfy $\sigma_i^M \geq m_{ii} - r_i$, where

$$r_i = \sum_{j=0, j\neq i}^{n} |m_{ij}| = \sum_{j=0, j\neq i}^{n} |-\beta b_{ij}| = -\beta b_{ii}. \tag{4.6}$$

Then we have $\sigma_i^M \geq m_{ii} - r_i = 1 - \beta b_{ii} + \beta b_{ii} = 1$. Therefore, the implicit Euler scheme with reflecting-reflecting boundary conditions is unconditionally stable.

Suppose that, instead of a reflecting condition, an absorbing condition at the left boundary is enforced by setting $b_{0j} = 0$ for all j. Then $r_0 = \sum_{j=1}^{n} b_{0j} = 0$, so $\sigma_0^M \geq m_{00} - r_0 = 1 - \beta b_{00} = 1$. For this case, all other eigenvalues satisfy the property $\sigma_i^M \geq 1$ as above, so the implicit Euler scheme is unconditionally stable. This argument follows in the same way when the right boundary condition is absorbing, so that $b_{nj} = 0$ for all j, and $\sigma_n^M \geq m_{nn} - r_n = 1 - \beta b_{nn} = 1$. Therefore, the implicit Euler scheme with any combination of reflecting and absorbing boundary conditions is unconditionally stable. □

REMARK 4.2. Since the matrix B^0 of (3.8) shares the properties of B that imply (4.6) in the proof of Theorem 4.2, the same argument results in the unconditional stability of the implicit Euler schemes for the centered normalized TFD equation.

REMARK 4.3. One could devise a Crank-Nicolson scheme with different combinations of reflecting and absorbing boundary conditions using a

similar approach to the one proposed in Section 3, and the resulting coefficient matrix would share the property of B (or B^0) that the row sums are less than or equal to zero, with non-negative off-diagonal entries and negative diagonal entries. Stability follows from the Gerschgorin circle theorem. For absorbing-absorbing boundary conditions, this was done in [3].

5. **Steady-state solutions**

In this section, we first compute the kernel of the NTRL derivative and then derive analytical steady-state solutions of the normalized TFD equation (2.7) with reflecting boundary conditions. A similar approach is applied to deriving the steady-state solution of the centered normalized model.

If $\lambda = 0$, steady-state solutions for one-sided fractional diffusion equations with reflecting boundary conditions were derived in [1, 2]. In particular, Baeumer et al. [1] showed that the steady-state solution of the one-sided fractional diffusion equation on $[0, 1]$ with unit mass and reflecting boundary conditions is $(\alpha-1)x^{\alpha-2}$. Steady-state solutions for two-sided fractional diffusion equations with different combinations of absorbing and reflecting boundary conditions were derived in [21], while the regularity of the two-sided steady-state solutions with absorbing-absorbing boundary conditions was investigated in Ervin et al. [14]. It was shown in [1, 2, 21] that the steady-state solutions of both one- and two-sided fractional diffusion equations using the RL derivative are not constant unless $\alpha = 2$, and instead have singularities at one or both boundaries.

We identify all steady-state solutions $u_\infty(x)$ (e.g., the null-space, or kernel) of the one-sided normalized tempered fractional diffusion equation:

$$\mathbb{D}_{0+}^{\alpha,\lambda} u_\infty(x) - \lambda^\alpha u_\infty(x) = 0 \tag{5.1}$$

on the interval $[L, R] = [0, 1]$.

Remark 5.1. We may choose the interval $[0, 1]$ without loss of generality, as a point x in $[0, 1]$ may be mapped to a point $y \in [L, R]$ using the transformation $y = x(R - L) + L$. This change of variables may be used to transform the results of this section so that they apply in any interval $[L, R]$.

Theorem 5.1. *Equation* (5.1) *for* $1 < \alpha < 2$ *has steady-state solutions*

$$u_\infty(x) = c_0 e^{-\lambda x}(\lambda x)^{\alpha-1} E_{\alpha,\alpha}((\lambda x)^\alpha) + c_1 e^{-\lambda x}(\lambda x)^{\alpha-2} E_{\alpha,\alpha-1}((\lambda x)^\alpha), \tag{5.2}$$

where c_0 *and* c_1 *are arbitrary real constants, and* $E_{\alpha,\beta}(x)$ *is the two-parameter Mittag-Leffler function*

$$E_{\alpha,\beta}(x) = \sum_{k=0}^{\infty} \frac{x^k}{\Gamma(\alpha k + \beta)} \tag{5.3}$$

with $\alpha > 0$ *and* $\beta \in \mathbb{C}$ [22, Equation (1.8.17)].

P r o o f. Using (2.3) and multiplying each side of (5.1) by $e^{\lambda x}$ and defining $w(x) = e^{\lambda x} u_\infty(x)$, (5.1) may be written as

$$\mathbb{D}^{\alpha}_{0+} w(x) - \lambda^\alpha w(x) = 0. \tag{5.4}$$

The kernel of the operator in Equation (5.4) is the two-dimensional space of functions of the form [22, Equation (4.2.44)]

$$w_0(x) = (\lambda x)^{\alpha-1} E_{\alpha,\alpha}((\lambda x)^\alpha),$$
$$w_1(x) = (\lambda x)^{\alpha-2} E_{\alpha,\alpha-1}((\lambda x)^\alpha),$$

so that $w(x) = c_0 w_0(x) + c_1 w_1(x)$. The result (5.2) then follows using the definition of $w(x)$. □

Proposition 5.1. *The functions* $u_0(x) = e^{-x} x^{\alpha-1} E_{\alpha,\alpha}(x^\alpha)$ *and* $u_1(x) = e^{-x} x^{\alpha-2} E_{\alpha,\alpha-1}(x^\alpha)$ *behave asymptotically as* $u_i(x) \sim 1/\alpha$ *as* $x \to \infty$ *for* $i = 0, 1$.

P r o o f. The asympototic behavior of $E_{\alpha,\beta}(x)$ as $x \to \infty$ for $1 < \alpha < 2$ is given by [22, Equation (1.8.27)]:

$$E_{\alpha,\beta}(x) \sim \frac{1}{\alpha} x^{(1-\beta)/\alpha} \exp\left(x^{1/\alpha}\right).$$

Hence

$$u_i(x) = e^{-x} x^\beta E_{\alpha,\beta+1}(x^\alpha) \sim e^{-x} \frac{x^\beta}{\alpha} (x^\alpha)^{(1-(\beta+1))/\alpha} \exp\left(x^{\alpha/\alpha}\right) \sim \frac{1}{\alpha}$$

for $i = 0$ or 1. □

Proposition 5.2. *For any* $x > 0$,

$$u_1(x) - u_0(x) = e^{-x} x^{\alpha-2} E_{\alpha,\alpha-1}(x^\alpha) - e^{-x} x^{\alpha-1} E_{\alpha,\alpha}(x^\alpha) > 0.$$

P r o o f. The two-parameter Mittag-Leffler function (5.3) satisfies [22, Equation (1.9.6)]

$$\left(\frac{d}{dx}\right)^m \left[x^{\beta-1} E_{\alpha,\beta}(x^\alpha)\right] = x^{\beta-m-1} E_{\alpha,\beta-m}(x^\alpha), \tag{5.5}$$

for $m \in \mathbb{N}$, $\alpha, \beta \in \mathbb{C}$, and $\mathrm{Re}(\alpha) > 0$. Setting $m = 1$ and $\beta = \alpha$ yields $\frac{d}{dx}\left[x^{\alpha-1} E_{\alpha,\alpha}(x^\alpha)\right] = x^{\alpha-2} E_{\alpha,\alpha-1}(x^\alpha)$. By the product rule,

$$\frac{d}{dx}\left[e^{-x}x^{\alpha-1}E_{\alpha,\alpha}(x^\alpha)\right] = -e^{-x}x^{\alpha-1}E_{\alpha,\alpha}(x^\alpha) + e^{-x}x^{\alpha-2}E_{\alpha,\alpha-1}(x^\alpha)$$
$$= u_1(x) - u_0(x).$$

It suffices to prove that the function $e^{-x}x^{\alpha-1}E_{\alpha,\alpha}(x^\alpha)$ is increasing. Choose $x_0, x_1 > 0$ such that $x_0 < x_1$. Then

$$e^{-x_1}x_1^{\alpha-1}E_{\alpha,\alpha}(x_1^\alpha) - e^{-x_0}x_0^{\alpha-1}E_{\alpha,\alpha}(x_0^\alpha)$$
$$> e^{-x_1}\left(x_1^{\alpha-1}E_{\alpha,\alpha}(x_1^\alpha) - x_0^{\alpha-1}E_{\alpha,\alpha}(x_0^\alpha)\right)$$
$$= e^{-x_1}\sum_{k=0}^{\infty}\frac{x_1^{\alpha-1}x_1^{\alpha k} - x_0^{\alpha-1}x_0^{\alpha k}}{\Gamma(\alpha k+\alpha)} > 0,$$

since $x^{\alpha k+\alpha-1}$ is increasing for $x > 0$ and $\Gamma(\alpha k+\alpha) > 0$ for any $\alpha \in (1,2)$ and any $k \geq 0$. Therefore, $e^{-x}x^{\alpha-1}E_{\alpha,\alpha}(x^\alpha)$ is increasing for $x > 0$. □

COROLLARY 5.1. *The steady-state solution of* (5.1) *that satisfies reflecting BCs with unit mass is*

$$u_\infty(x) = \frac{e^{-\lambda x}}{K}\left[(\lambda x)^{\alpha-2}E_{\alpha,\alpha-1}((\lambda x)^\alpha) - (\lambda x)^{\alpha-1}E_{\alpha,\alpha}((\lambda x)^\alpha)\right] \tag{5.6}$$

with normalization constant

$$K = e^{-\lambda}\lambda^{\alpha-2}E_{\alpha,\alpha}(\lambda^\alpha). \tag{5.7}$$

P r o o f. Observe that $u_\infty(x) = c_0u_0(\lambda x) + c_1u_1(\lambda x)$ for any $\lambda > 0$. Also, note that $u_1(x) > u_0(x)$ for all $x > 0$ according to Proposition 5.2. By Proposition 5.1, the only linear combination of $u_0(x)$ and $u_1(x)$ that is both non-negative for all $x > 0$ and that approaches zero as $x \to \infty$ is $(1/K)(u_1(x) - u_0(x))$ for some constant $K > 0$. Hence, the only choice of c_0 and c_1 that ensures $u_\infty(x)$ in (5.2) is non-negative on $[0,1]$ for any choice of λ is $c_1 = -c_0 = (1/K) > 0$, where K is chosen to be (5.7) to ensure unit mass:

$$K = \int_0^1 e^{-\lambda y}\left((\lambda y)^{\alpha-2}E_{\alpha,\alpha-1}(\lambda y) - (\lambda y)^{\alpha-1}E_{\alpha,\alpha}(\lambda y)\right)dy$$
$$= \int_0^1 \frac{1}{\lambda}\frac{d}{dy}\left[e^{-\lambda y}(\lambda y)^{\alpha-1}E_{\alpha,\alpha}((\lambda y)^\alpha)\right]dy$$
$$= e^{-\lambda}\lambda^{\alpha-2}E_{\alpha,\alpha}(\lambda^\alpha),$$

where (5.5) is used in the second line. □

REMARK 5.2. Recall that the centered model (2.11) is derived from the normalized model by computing the mean of the normalized model

solution via the Fourier transform. Restricting to the bounded domain yields a different mean depending on the size of the interval. We analytically derive the mean μ of the steady-state solution in the interval $[0,1]$ using the explicit form of $u_\infty(x)$ in Equation (5.6):

$$\begin{aligned}\mu &= \int_0^1 x u_\infty(x)\,dx \\ &= \int_0^1 \frac{x e^{-\lambda x}}{K}\left[(\lambda x)^{\alpha-2}E_{\alpha,\alpha-1}((\lambda x)^\alpha) - (\lambda x)^{\alpha-1}E_{\alpha,\alpha}((\lambda x)^\alpha)\right]\,dx \\ &= \sum_{j=0}^{\infty}\frac{\lambda^{\alpha j}}{E_{\alpha,\alpha}(\lambda^\alpha)}\left[(\alpha j+\alpha-1)E_{1,\alpha j+\alpha+1}(\lambda) - \lambda(\alpha j+\alpha)E_{1,\alpha j+\alpha+2}(\lambda)\right],\end{aligned} \tag{5.8}$$

where we used the identity [17, Equation (4.4.6)]

$$\int_0^1 x^\gamma e^{-\lambda x}\,dx = e^{-\lambda}\Gamma(\gamma+1)E_{1,\gamma+2}(\lambda).$$

PROPOSITION 5.3. *As $\lambda \to 0$, the steady-state solution* (5.6) *converges pointwise to the untempered steady-state solution $u_\infty(x) \to (\alpha-1)x^{\alpha-2}$ for all $x > 0$.*

P r o o f. Taking the limit of $u_\infty(x)$ as $\lambda \to 0$ yields

$$\begin{aligned}\lim_{\lambda\to 0} u_\infty(x) &= \lim_{\lambda\to 0}\frac{e^{-\lambda x}(\lambda x)^{\alpha-2}E_{\alpha,\alpha-1}((\lambda x)^\alpha) - e^{-\lambda x}(\lambda x)^{\alpha-1}E_{\alpha,\alpha}((\lambda x)^\alpha)}{e^{-\lambda}\lambda^{\alpha-2}E_{\alpha,\alpha}(\lambda^\alpha)} \\ &= \lim_{\lambda\to 0}\frac{e^{-\lambda x+\lambda}x^{\alpha-2}E_{\alpha,\alpha-1}((\lambda x)^\alpha) - e^{-\lambda x+\lambda}\lambda x^{\alpha-1}E_{\alpha,\alpha}((\lambda x)^\alpha)}{E_{\alpha,\alpha}(\lambda^\alpha)} \\ &= \frac{x^{\alpha-2}E_{\alpha,\alpha-1}(0) - 0}{E_{\alpha,\alpha}(0)} = x^{\alpha-2}\frac{\Gamma(\alpha)}{\Gamma(\alpha-1)} = (\alpha-1)x^{\alpha-2},\end{aligned}$$

where $E_{\alpha,\beta}(0) = 1/\Gamma(\beta)$ is used in the fourth line. □

REMARK 5.3. The steady-state solution of the centered normalized model (2.11) satisfies

$$\mathbb{D}_{0^+}^{\alpha,\lambda}u_\infty(x) - \lambda^\alpha u_\infty(x) - \alpha\lambda^{\alpha-1}\partial_x u_\infty(x) = 0, \tag{5.9}$$

for $0 \le x \le 1$. Defining the function $w(x) = e^{\lambda x}u_\infty(x)$ yields

$$\mathbb{D}_{0^+}^{\alpha}w(x) - \lambda^\alpha(1-\alpha)w(x) - \alpha\lambda^{\alpha-1}\partial_x w(x) = 0. \tag{5.10}$$

The solutions of (5.10) are reported in Kilbas et al. [22, Corollary 5.3] as an infinite series of Wright functions ${}_1\Psi_1(\mathrm{x})$ [22, Equation (1.11.14)].

6. **Numerical examples**

Figure 1 compares numerical solutions of the one-sided tempered fractional diffusion equation with reflecting boundary conditions using order $\alpha = 1.3$ in panel 1(a) and order $\alpha = 1.8$ in panel 1(b) using a tempering parameter of $\lambda = 1$ with the analytical steady-state solution (5.6). The initial condition $u(x, 0) = u_0(x)$ is a tent function with unit mass

$$u_0(x) = \begin{cases} 25x - 7.5 & 0.3 < x < 0.5, \\ -25x + 17.5 & 0.5 < x < 0.7, \\ 0 & \text{otherwise.} \end{cases} \tag{6.1}$$

A total of 401 grid-points were used with the implicit Euler scheme using a time-step of $\Delta t = 0.01$, while the steady-state solution (5.6) was evaluated using freely available codes for the Mittag-Leffler function [31]. The numerical solution at time $t = 1$ and the steady-state solution (5.6) agree well, indicating that the long-time numerical solutions are consistent with the analytical steady-state solution.

Remark 6.1. Like the one-sided fractional steady-state solution, (5.2) is singular at $x = 0$ and smooth at $x = 1$. The tempered fractional derivative, like the Riemann-Liouville fractional derivative, has a leftward advection component that causes the plume's center of mass to advect towards the left boundary. To see why the leftward component dominates the long jumps to the right, consider the values of the coefficients in the Grünwald-Letnikov discretization where $\alpha = 1.5$. Given a point x_j in the domain, recall that each g_i^α determines the amount of mass moving from x_j to x_{j-i+1} (if $i \neq 1$). As $n \to \infty$, $\sum_{i=2}^{n} g_i^\alpha$ converges to $\alpha - 1$, which is less than $g_0^\alpha = 1$. As g_0^α determines the proportion of mass advecting to the left of x_j, and $\{g_i^\alpha\}_{i \geq 2}$ determines the proportion of mass jumping to the right of x_j, the leftward movement of mass dominates the overall evolution of the solution. Hence, over time, the mass accumulates at the left boundary and forms a singularity. Compared with the Riemann-Liouville derivative, tempering the operator does not increase the regularity of the steady-state solution. Since this singular behavior is not observed either experimentally or in the field, alternative definitions of the tempered fractional derivative should be analyzed with discrete reflecting boundary conditions. In the non-tempered case, diffusion equations based on the mixed-Caputo, also known as Patie-Simon, derivative have constant steady-state solutions [2, 21]. The tempered model discussed in [42], which was analyzed using a Lagrangian solver, may be written in a mixed-Caputo form and may be discretized using the numerical methods presented in Section 3.

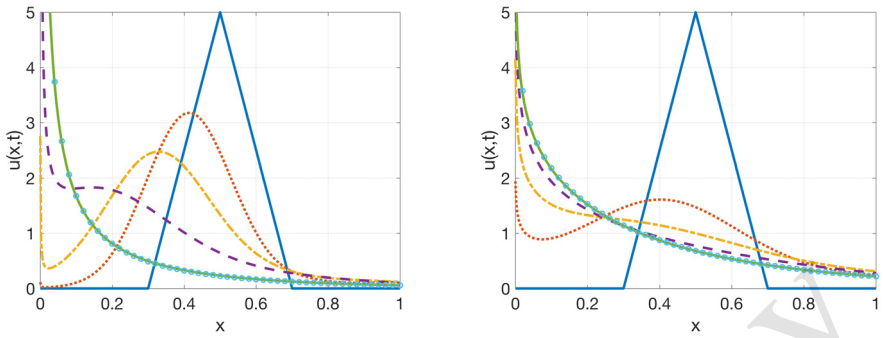

(a) $\alpha = 1.3$ (b) $\alpha = 1.8$

FIGURE 1. Comparison of numerical solutions (lines) and steady-state solution given by (5.6) (circles) for (a) $\alpha = 1.3$ and (b) $\alpha = 1.8$ using a tempering parameter of $\lambda = 1$ and times $t = 0$ (solid tent function), 0.05 (dotted), 0.1 (dash-dotted), 0.2 (dashed), and 1 (solid green). The steady-state solution is plotted using circles.

REMARK 6.2. Spectral methods are able to accurately capture the singular derivatives of solutions for fractional diffusion models with Dirichlet boundary conditions [40, 38, 8]. Most spectral methods for fractional diffusion models are formulated by choosing a set of spatial basis functions $\{\phi_m(x)\}_{m=1}^M$ that satisfy the prescribed boundary conditions and approximating of the solution $u(x,t) \approx \sum_{m=1}^M a_m(t)\phi_m(x)$, where $\{a_m(t)\}$ are time-dependent coefficients determined by the numerical method. Deriving appropriate basis functions $\{\phi_m(x)\}$ for tempered diffusion that are consistent with the reflecting boundary condition is challenging, requiring analysis of the boundary operator, and remains an open problem.

Figure (2) displays the implicit Euler solutions of Equation (2.7) in plots (a)–(c) and Equation (2.11) in plots (d)–(f) with $\alpha = 1.5$ using the initial condition (6.1) and reflecting conditions at each boundary. The domain is discretized by 401 grid points and $\Delta t = 0.01$ with $\lambda = 0.1, 1$, and 10 at times $t = 0, 0.05, 0.1, 0.2, 0.5$, and 1. The solutions at $t = 1$ agree well with the analytical steady-state solution given by (5.2). As λ increases, mass is more concentrated near the left boundary, which means that increasing the tempering parameter increases the strength of the singularity at the left boundary. This behavior is caused by the increase in leftward diffusion as λ increases.

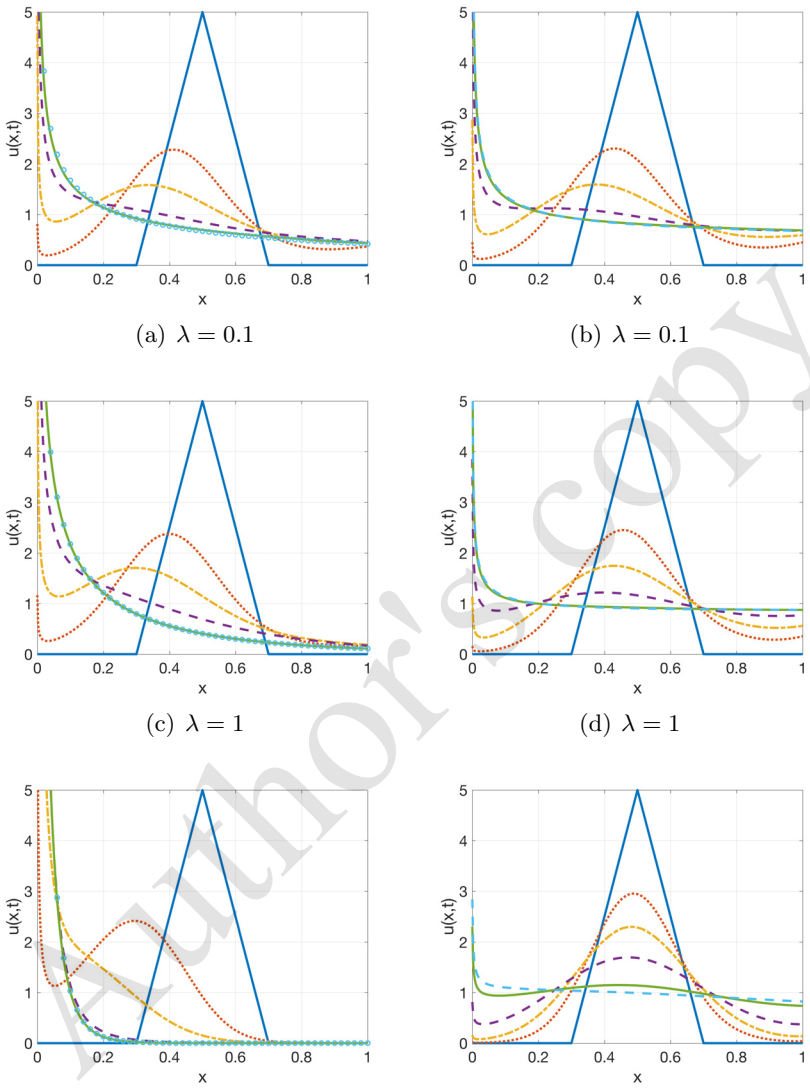

(a) $\lambda = 0.1$ (b) $\lambda = 0.1$

(c) $\lambda = 1$ (d) $\lambda = 1$

(e) $\lambda = 10$ (f) $\lambda = 10$

FIGURE 2. Implicit Euler solutions of the normalized TFD equation (2.7) (plots (a), (c), and (e)) and the centered normalized TFD equation (2.11) (plots (b), (d), and (f)) with reflecting-reflecting boundary conditions for different values of λ with $\alpha = 1.5$, 401 grid points, and $\Delta t = 0.01$. The initial condition is the tent function (6.1) represented as a solid curve in both plots. The solutions are plotted at times $t = 0$ (solid tent function), 0.05 (dotted), 0.1 (dash-dotted), 0.2 (dashed), and 1 (solid green). The steady-state solution is plotted using circles.

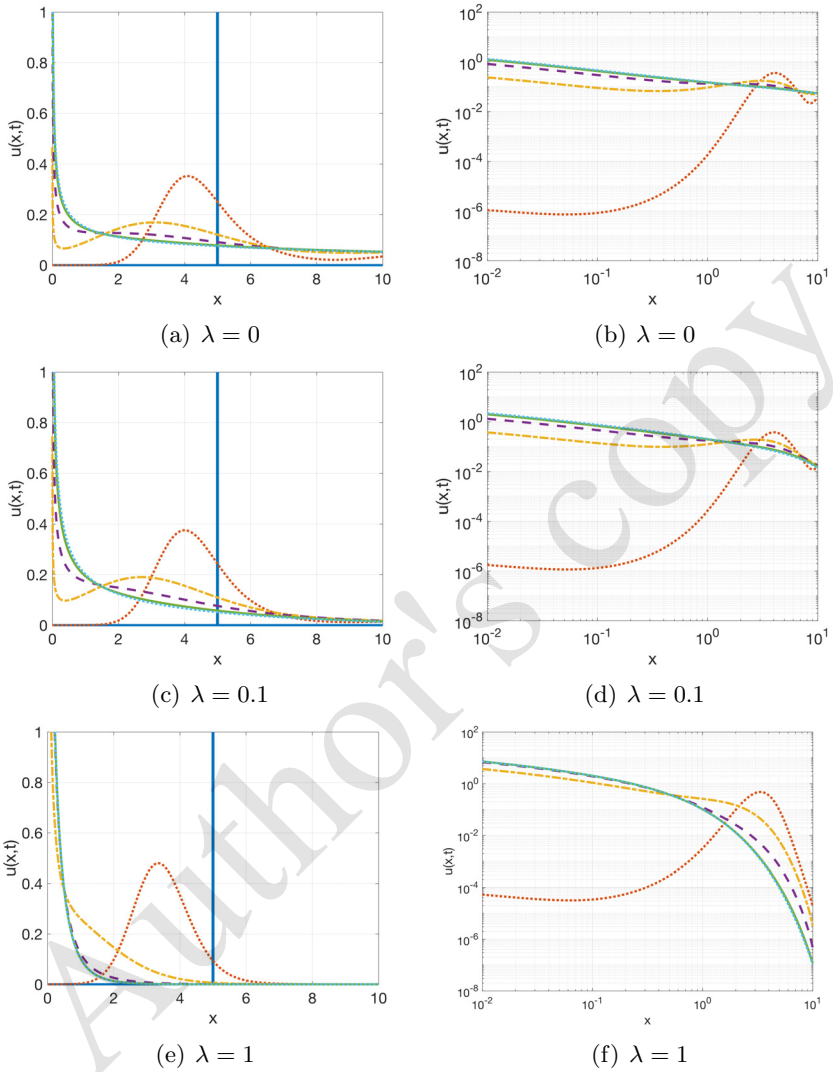

(a) $\lambda = 0$ (b) $\lambda = 0$

(c) $\lambda = 0.1$ (d) $\lambda = 0.1$

(e) $\lambda = 1$ (f) $\lambda = 1$

FIGURE 3. Implicit Euler solutions of the normalized TFD equation (2.7) with reflecting-reflecting boundary conditions for different values of λ with $\alpha = 1.5$, 1001 grid points, and $\Delta t = 0.01$. Plots (a), (c), and (e) have linear-linear scale, and plots (b), (d), and (f) represent the same functions in log-log scale. The initial condition is the delta function represented as a solid curve. The solutions are plotted at times $t = 0$ (solid), 1 (dotted), 3 (dash-dotted), 5 (dashed), 8 (solid green), and 1 (dotted blue).

In Figure (3), the effect of the tempering parameter on solutions of the normalized TFD equation can be observed. In the log-log plots of subfigures (d) and (f), the effect of the tempering of the long jumps to the right is visible, since the concentration of mass at the right boundary decreases as λ increases. Furthermore, particularly in panel (e) with $\lambda = 0.1$, the power law behavior in the solutions is clearly visible, with a transition to exponential behavior near $x = 1/\lambda$.

Centered Normalized Model Means							
	Time t						
λ	0	0.05	0.1	0.2	0.5	1	2
0.1	0.5	0.4745	0.4485	0.4175	0.3958	0.3905	0.3898
1.0	0.5	0.4926	0.4826	0.4676	0.4554	0.4527	0.4519
10.0	0.5	0.4987	0.4970	0.4930	0.4850	0.4799	0.4766

Normalized Model Means							
	Time t						
λ	0	0.05	0.1	0.2	0.5	1	2
0.1	0.5	0.4516	0.4068	0.3562	0.3193	0.3114	0.3108
1.0	0.5	0.4191	0.3459	0.2600	0.1954	0.1847	0.1841
10.0	0.5	0.2633	0.0926	0.0268	0.0246	0.0246	0.0246

TABLE 1. Means for the normalized and centered normalized solutions with $\alpha = 1.5$ and tempering parameters $\lambda = 0.1$, 1.0, and 10.0. Numerical solutions were computed using the implicit Euler schemes with $\Delta t = 0.001$ and $n = 801$ grid points on the interval $[0, 1]$.

One benefit of the centered model used in [3] is that, on the real line, the mean of $p_{\lambda,0}(x, t)$ is zero for all $t \geq 0$. As the model has been restricted to a bounded domain, the third (centering) term in the CNTRL (2.11) no longer centers the mean to zero. However, while the centering term no longer represents the exact mean of the plume on the bounded domain, one can notice from Table 1 that the mean remains closer to the center than in the normalized model (2.7), especially for large values of λ. Note that the mean is different from the peak of the solution curves, which represents the mode.

Given the solution of the centered normalized TFD equation $u(x, t)$ on the domain $[0, 1]$, the solution means are numerically approximated for different values of t as $\int_0^1 xu(x, t)\, dx \approx h \sum_{i=0}^{n} x_i u(x_i, t)$. Table 1 displays the means at different times for $\alpha = 1.5$ and tempering parameters $\lambda =$

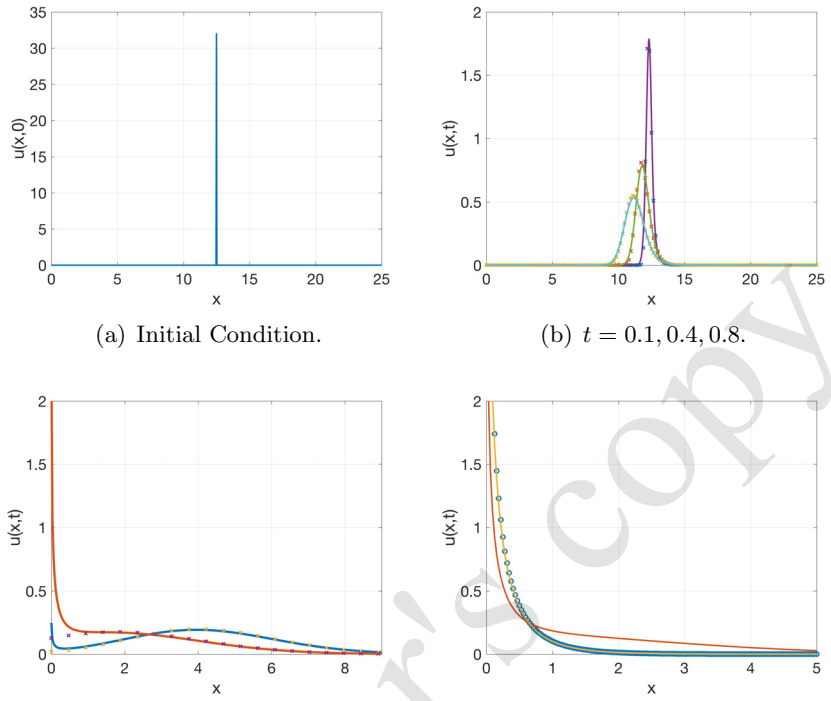

(a) Initial Condition. (b) $t = 0.1, 0.4, 0.8$.

(c) $t = 5.5$ and 7. (d) $t = 8, 15$ and steady-state.

FIGURE 4. We solve the normalized TFD equation (2.7) using the implicit Euler method with $\alpha = 1.5$, $\lambda = 1$, $n = 801$ grid points, and $\Delta t = 0.01$ on the domain $[0, 25]$. (a) The impulsive initial condition; (b) the solid curves are the numerical solutions at times $t = 0.1, 0.4, 0.8$, and the 'x' markers represent the tempered stable densities at the same times; (c) the solid curves are the numerical solutions at times $t = 5.5, 7$, and the 'x' markers represent the tempered stable densities at the same times; (d) the solid curves are the numerical solutions at times $t = 8, 15$, and the circle markers represent the analytical steady-state solution.

0.1, 1.0, and 10.0. The normalized model means in Table 1 at time $t = 2$ were compared to the analytical mean μ given by (5.8), and the two computations agreed up to three digits for each value of λ. We also include the means of the normalized model given the same parameter values for comparison. While the mean of the solution of the centered model is not

exactly centered in the interval, it is much closer to the center relative to the mean of the normalized model solutions.

On the real line, given any initial condition, the solution at any time t is a spatial convolution of a fundamental solution (point-source solution) with the initial condition. Note that the fundamental solutions on the real line, $p_\lambda(x,t)$ given by (2.8) and $p_{\lambda,0}(x,t)$ given by (2.12), are products of exponential functions and maximally skewed stable densities $f_\alpha(x,t)$. Since all stable densities are smooth [46], both $p_\lambda(x,t)$ and $p_{\lambda,0}(x,t)$ are smooth for all t. By properties of convolutions, any solution on the real line for $t > 0$ will also be smooth given any initial condition. However, the introduction of the reflecting boundary alters the regularity of the solution space. Figure 4 suggests that for any initial condition, the numerical solution is a singular function for $t > 0$. Figure 4 shows the evolution of numerical solutions of (2.7) from an impulse initial condition to the steady-state solution (at time $t = 15$). The initial condition is discretized as $u(x = 12.5) = 1/h$, which is consistent with $u_0(x) = \delta(x - 12.5)$. The solution is computed on the domain $[0, 25]$ using the implicit Euler scheme with $\alpha = 1.5$, $\lambda = 1$, $n = 801$ grid points, and $\Delta t = 0.01$. For small times ($t = 0.1, 0.4$, and 0.8), the numerical solution is close to the smooth tempered stable density $p_\lambda(x,t)$, as the boundary conditions have not yet affected the solution. The relative L^∞-norm error for times $t = 0.1, 0.4$, and 0.8 are $0.0430, 0.0124$, and 0.0074, respectively. Note, however, that the purpose of Figure 4 is to qualitatively show how the solution transitions from a stable density to the steady state, so approximating the solution with accuracy is not critical here. The tempered α-stable density (2.8) was computed using a freely available MATLAB code [37] for the evaluation of the stable densities $f_\alpha(x,t)$. For times $t = 5.5$ and 7, a singularity forms at the boundary, which evolves into the singular steady-state solution in Figure 4(d).

When both boundary conditions are absorbing, both implicit and explicit schemes converge with rate $\mathcal{O}(h)$ if the solution is sufficiently smooth [3, Proposition 3]. However, when the source function is zero, the solutions of the normalized and centered models are weakly singular (i.e., the first derivative is singular) at the left boundary, which leads to a degradation in the rate of convergence, as the singularity is not faithfully captured with a uniform grid. When the left boundary condition is reflecting, the solution itself is singular at $x = 0$. One approach to address the degradation of the convergence rate is to use non-uniform grid spacing. Near $x = 0$, additional refinement may capture the singular solution with greater fidelity. Preliminary work exists to discretize Caputo fractional derivatives with non-uniform grids [15, 32, 33, 44] and Riemann-Liouville fractional derivatives [25] using spectral finite elements on graded meshes.

Since the explicit form of this boundary condition is quite difficult to analyze, we provide numerical convergence studies, demonstrating that the convergence rates using a reflecting boundary condition on one endpoint are the same as using absorbing boundary conditions at both endpoints. In Figure 5, convergence results for both absorbing-absorbing and absorbing-reflecting boundary conditions applied to the normalized model are compared. The error is computed in the relative L^∞-norm using a reference solution u_{ref}, which is computed using the implicit Euler scheme with $\Delta t = 0.001$ on a fine grid with $n = 2401$ points and initial condition (6.1). The relative L^∞-error is given by $\|u_h - u_{ref}\|_{L^\infty}/\|u_{ref}\|_{L^\infty}$, where the numerical solution u_h is computed with the explicit or implicit Euler method with grid spacing $h = 1/200, 1/400, 1/800$, and $1/1600$. In each case, the fractional order is $\alpha = 1.5$ and the tempering parameter is $\lambda = 1$. The implicit Euler solutions are computed using time step $\Delta t = 0.001$, and the explicit Euler solutions are computed with time step $\Delta t = 5 \times 10^{-6}$.

First, the relative L^∞-error of the implicit and explicit Euler schemes for the normalized model with absorbing-absorbing boundary conditions is plotted in panels 5(c)-5(e) at times $t = 0.2$ and 1, with a dashed line representing $\mathcal{O}(h)$ convergence rate for reference. The reference solution u_{ref} is plotted in panel 5(a). One can observe that the convergence rate is degraded slightly from $\mathcal{O}(h)$ due to the weak singularity at $x = 0$. The solutions computed with $n = 1601$ grid points capture the singularity with accuracy close to that of the reference solution, so the error decreases with a higher rate between the smallest two values of h. A similar trend is apparent in the error plots in panels 5(d)-5(f), where the boundary conditions are absorbing-reflecting. In this case, the weak singularity at $x = 0$ is similar to the absorbing-absorbing boundary conditions example, so the two convergence studies are comparable. The reflecting boundary condition at $x = 1$ does not degrade the convergence rate from that of the absorbing-absorbing boundary condition case.

Next, convergence results are compared for different values of α in the normalized model. In Figures 6(a) and 6(b), numerical solutions for the normalized model with $\alpha = 1.2$ and $\alpha = 1.8$, respectively, are plotted. For the smaller value of α, the singular behavior of the derivative of $u(x, t)$ at the left boundary is more severe than in the cases with $\alpha = 1.5$ or $\alpha = 1.8$. This behavior degrades the convergence rates, as can be seen in Figures 6(c) and 6(e). Furthermore, approximations of (2.7) with larger values of α correspond with errors that converge like $\mathcal{O}(h)$. The centered model solutions exhibit similar behavior near the left boundary for different values of α.

In Figure 7, convergence results for the centered model with both absorbing-absorbing and absorbing-reflecting conditions are compared. In this model, no weak singularity forms at the left boundary for the times considered (see panels 7(a) and 7(b)), so one can observe that the relative L^∞-error converges with a rate approximately $\mathcal{O}(h)$. The reference solutions are again computed on $n = 2401$ grid points, and all other parameters are the same as in the convergence studies of Figure 5. Comparing the results for each set of boundary conditions demonstrates that the convergence rate is not degraded by the reflecting boundary condition.

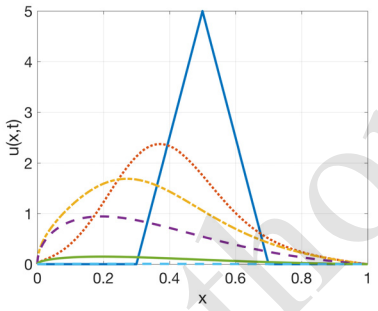

(a) Absorbing-absorbing BCs

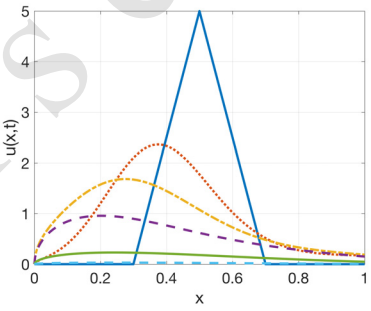

(b) Absorbing-reflecting BCs

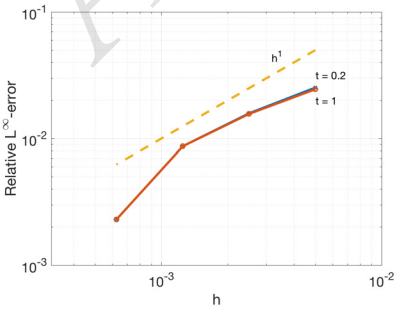

(c) Implicit Euler error

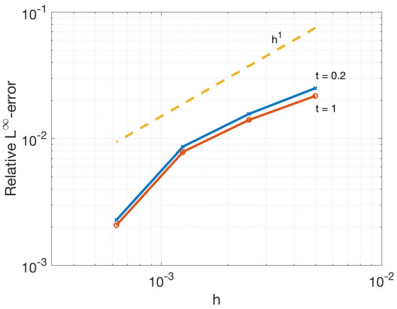

(d) Implicit Euler error

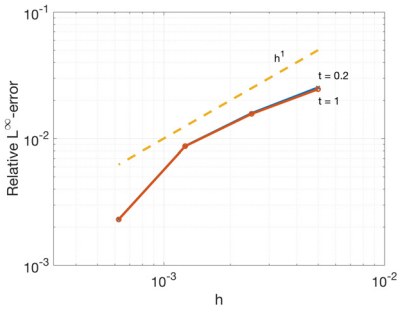

(e) Explicit Euler error

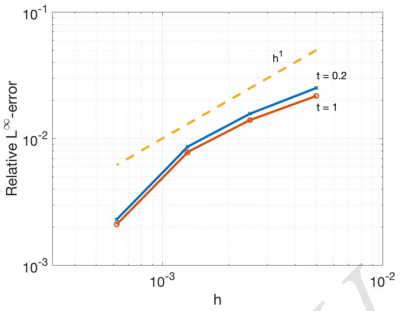

(f) Explicit Euler error

FIGURE 5. All plots above reference the normalized model (2.7) and use parameters $\alpha = 1.5$ and $\lambda = 1$. Errors are computed at times $t = 0.2$ and 1 and are plotted in log-log scale. Absorbing-absorbing BCs are used in the left column of plots and absorbing-reflecting BCs are used in the right column. (a) Reference solutions computed using the implicit Euler method with $n = 2401$, $\Delta t = 0.001$, and initial condition (6.1) plotted for times $t = 0, 0.1, 0.2, 0.5, 0.8,$ and 1. (b) Reference solutions computed using the implicit Euler method with the same paramters. (c) Implicit Euler error with $\Delta t = 0.001$. The error curves overlay each other. (d) Implicit Euler error with $\Delta t = 0.001$. (e) Explicit Euler error with $\Delta t = 5 \times 10^{-6}$. The error curves overlay each other. (f) Explicit Euler error with $\Delta t = 5 \times 10^{-6}$.

7. Summary

In this work, we have developed stable explicit and implicit Euler methods for tempered fractional diffusion models with discrete reflecting or absorbing boundary conditions. The analytical steady-state solution for the tempered fractional diffusion equation was derived and compared to numerical solutions, and the steady-state solution of a centered model was discussed. We compared three different tempered fractional diffusion models and identified two models that conserve mass: the normalized tempered model (2.7) and the center normalized tempered model (2.11). Convergence of the reflecting Euler schemes was studied by comparing numerical solutions.

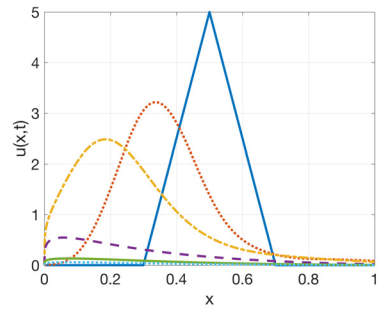

(a) Reference solution, $\alpha = 1.2$

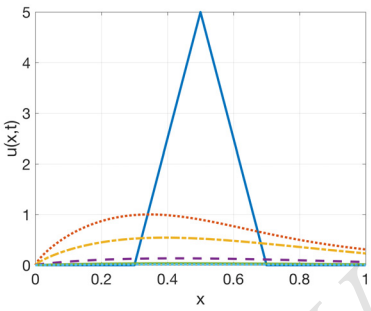

(b) Reference solution, $\alpha = 1.8$

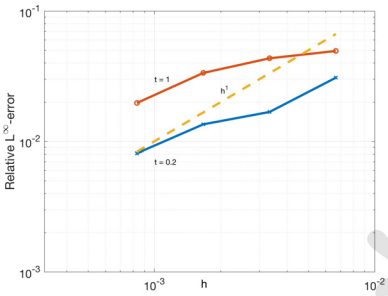

(c) Implicit Euler error, $\alpha = 1.2$

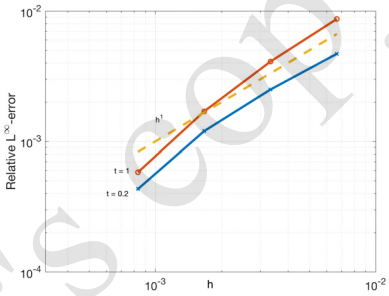

(d) Implicit Euler error, $\alpha = 1.8$

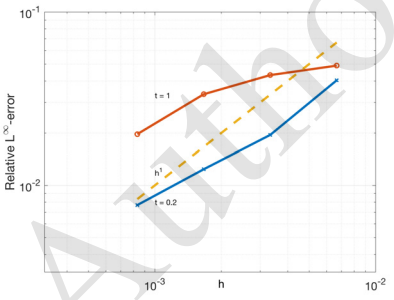

(e) Explicit Euler error, $\alpha = 1.2$

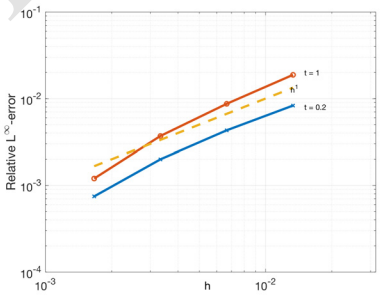

(f) Explicit Euler error, $\alpha = 1.8$

FIGURE 6. All plots above reference the normalized model (2.7) with absorbing-reflecting boundary conditions, $\lambda = 1$, and initial condition (6.1). Errors are computed at times $t = 0.2$ and 1. The left column shows results for $\alpha = 1.2$ and the right column shows results for $\alpha = 1.8$. (a - b) Reference solutions computed with the implicit Euler method with $n = 1201$ grid points, $\Delta t = 0.001$ for times $t = 0, 0.1, 0.2, 0.5, 0.8$, and 1 with $\alpha = 1.2$ and $\alpha = 1.8$, respectively. (c - d) Implicit Euler error with $\Delta t = 0.01$ and $\Delta t = 0.001$, respectively. (e - f) Explicit Euler error with $\Delta t = 5\times10^{-5}$ and $\Delta t = 1\times10^{-6}$, respectively.

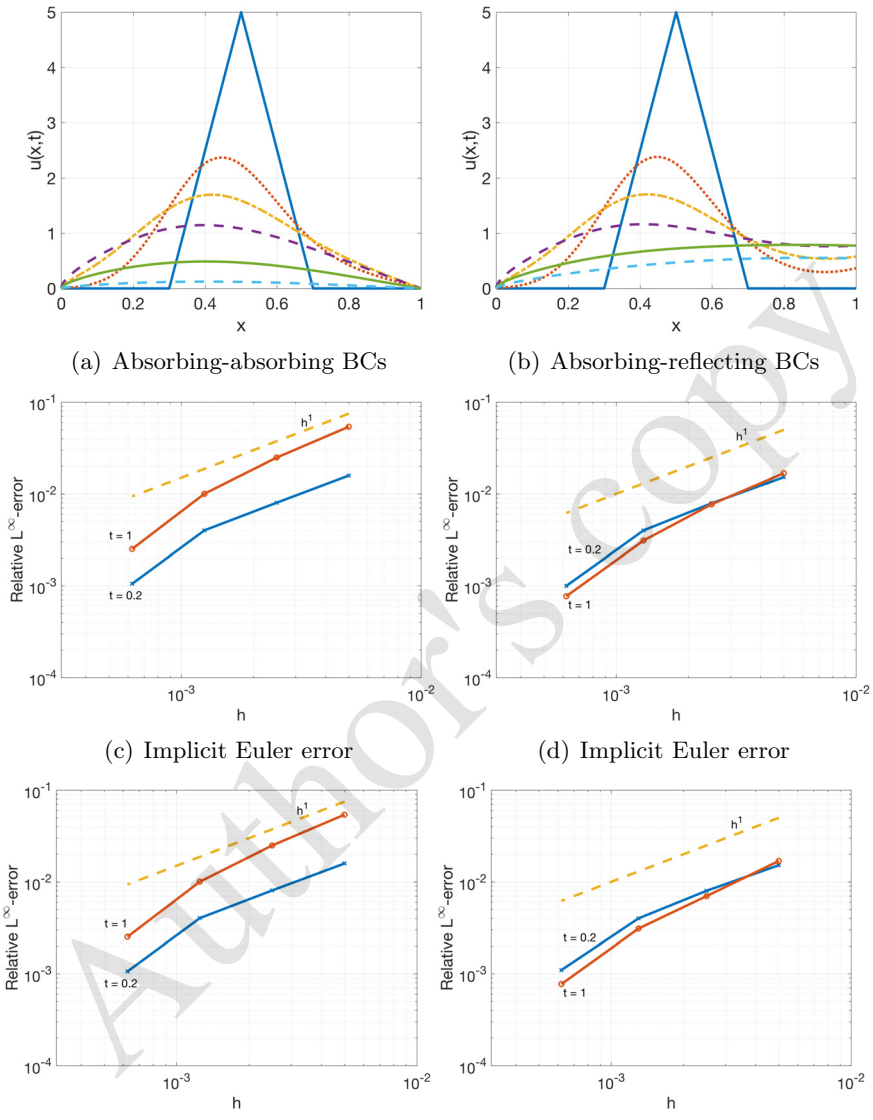

(a) Absorbing-absorbing BCs (b) Absorbing-reflecting BCs

(c) Implicit Euler error (d) Implicit Euler error

(e) Explicit Euler error (f) Explicit Euler error

FIGURE 7. All plots above reference the centered model (2.11) with $\alpha = 1.5$, $\lambda = 1$, and initial condition (6.1). The left column shows results for absorbing-absorbing BCs and the right column show results for absorbing-reflecting BCs. (a - b) Reference solutions computed with the implicit Euler method with $n = 2401$ grid points, $\Delta t = 0.001$, and times $t = 0, 0.05, 0.1, 0.2, 0.5$, and 1. (c - d) Implicit Euler error with $\Delta t = 0.001$. (e - f) Explicit Euler error with $\Delta t = 5 \times 10^{-6}$.

Acknowledgments

We would like to thank Harish Sankanarayanan (Department of Statistics and Probability, Michigan State University) for the fruitful discussions and suggestions for improving the manuscript. This work was supported by the OSD/ARO/MURI on "Fractional PDEs for Conservation Laws and Beyond: Theory, Numerics and Applications" (W911NF-15-1-0562). Kelly acknowledges support of the Chief of Naval Research via the base 6.1 support program.

References

[1] B. Baeumer, M. Kovács, M. M. Meerschaert, H. Sankaranarayanan, Boundary conditions for fractional diffusion. *J. of Computational and Applied Mathematics* **336** (2018), 408–424.

[2] B. Baeumer, M. Kovács, H. Sankaranarayanan, Fractional partial differential equations with boundary conditions. *J. of Differential Equations* **264** (2018), 1377–1410.

[3] B. Baeumer, M. M. Meerschaert, Tempered stable Lévy motion and transient superdiffusion. *J. of Computational and Applied Mathematics* **233**, No 10 (2010), 2438–2448.

[4] D. M. Benson, R. Schumer, M. M. Meerschaert, S. W. Wheatcraft, Fractional dispersion, Lévy motion, and the MADE tracer tests. *Transport in Porous Media* **42** (2001), 211–240.

[5] R. Bruno, L. Sorriso-Valvo, V. Carbone, B. Bavassano, A possible truncated-Lévy-flight statistics recovered from interplanetary solar-wind velocity and magnetic-field fluctuations. *EPL (Europhysics Letters)* **66**, No 1 (2004), 146–152.

[6] D. del Castillo-Negrete, Fractional diffusion models of nonlocal transport. *Physics of Plasmas* **13** (2006), No 082308; DOI: 10.1063/1.2336114.

[7] P. Chakraborty, M. M. Meerschaert, C. Y. Lim, Parameter estimation for fractional transport: A particle-tracking approach. *Water Resources Research* **45**, No 10 (2009), W10415.

[8] S. Chen, J. Shen, and L.-L. Wang, Laguerre functions and their applications to tempered fractional differential equations on infinite intervals. *J. of Scientific Computing* **74**, No 3 (2018), 1286–1313; DOI:10.1007/s10915-017-0495-7.

[9] M. Dehghan, M. Abbaszadeh, and W. Deng, Fourth-order numerical method for the space–time tempered fractional diffusion-wave equation. *Applied Mathematics Letters* **73** (2017), 120–127.

[10] W. Deng, B. Li, W. Tian, P. Zhang, Boundary problems for the fractional and tempered fractional operators. *Multiscale Modeling & Simulation* **16**, No 1 (2018), 125–149; DOI:10.1137/17M1116222.

[11] W. Deng and Z. Zhang, Variational formulation and efficient implementation for solving the tempered fractional problems. *Numerical Methods for Partial Differential Equations* **34**, No 4 (2018), 1224–1257; DOI:10.1002/num.22254.

[12] K. Diethelm, *The Analysis of Fractional Differential Equations*. Springer-Verlag, Berlin (2010).

[13] B. Dubrulle, J.-P. Laval, Truncated Lévy laws and 2d turbulence. *The European Physical J. B - Condensed Matter and Complex Systems* **4**, No 2 (1998), 143–146; DOI: 10.1007/s100510050362.

[14] V. Ervin, N. Heuer, J. Roop, Regularity of the solution to 1-d fractional order diffusion equations. *Mathematics of Computation* **87** (2018), 2273–2294; DOI:10.1090/mcom/3295.

[15] R. Fazio, A. Jannelli, S. Agreste, A finite difference method on non-uniform meshes for time-fractional advection-diffusion equations with a source term. *Applied Sciences* **8**, No 6 (2018), 960; DOI:10.3390/app8060960.

[16] W. Feller, *An Introduction to Probability Theory and Its Applications*. 2nd Edition, Vol. II, Wiley, New York (1971).

[17] R. Gorenflo, A. A. Kilbas, F. Mainardi, S. V. Rogosin, *Mittag-Leffler Functions, Related Topics and Applications*. Springer Inc., Berlin (2014).

[18] E. Isaacson, H. Keller, *Analysis of Numerical Methods*. John Wiley & Sons Inc., New York (1966).

[19] R. Jha, P. K. Kaw, D. R. Kulkarni, J. C. Parikh, Evidence of Lévy stable process in tokamak edge turbulence. *Physics of Plasmas* **10**, No 3 (2003), 699–704.

[20] J. F. Kelly, D. Bolster, M. M. Meerschaert, J. D. Drummond, A. I. Packman, FracFit: A robust parameter estimation tool for fractional calculus models. *Water Resources Research* **53**, No 3 (2017), 2559–2567.

[21] J. F. Kelly, H. Sankaranarayanan, M. M. Meerschaert, Boundary conditions for two-sided fractional diffusion. *J. of Computational Physics* **376** (2019), 1089–1107.

[22] A. A. Kilbas, H. M. Srivastava, J. J. Trujillo, *Theory and Applications of Fractional Differential Equations*. Vol. 204, Elsevier Science Ltd., Amsterdam (2006).

[23] C. Li, W. Deng, High order schemes for the tempered fractional diffusion equations. *Advances in Computational Mathematics* **42**, No 3 (2016), 543–572.

[24] C. Li, W. Deng, L. Zhao, Well-posedness and numerical algorithm for the tempered fractional ordinary differential equations. *Discrete & Continuous Dynamical Systems-B* **24**, No 4 (2019), 1989–2015.

[25] X. Li, Z. Mao, F. Song, H. Wang, and G. E. Karniadakis, A fast solver for spectral element approximation applied to fractional differential equations using hierarchical matrix approximation. *arXiv Preprint*: arXiv:1808.02937 (Aug. 2018).

[26] R. N. Mantegna, H. E. Stanley, Scaling behaviour in the dynamics of an economic index. *Nature* **376**, No 46 (1995), 46–49.

[27] M. Meerschaert, A. Sikorskii, *Stochastic Models for Fractional Calculus*. 2nd Edition, De Gruyter, Berlin (2019).

[28] M. M. Meerschaert, C. Tadjeran, Finite difference approximations for fractional advection–dispersion flow equations. *J. of Computational and Applied Mathematics* **172**, No 1 (2004), 65–77.

[29] M. M. Meerschaert, C. Tadjeran, Finite difference approximations for two-sided space-fractional partial differential equations. *Applied Numerical Mathematics* **56**, No 1 (2006), 80–90.

[30] M. M. Meerschaert, Y. Zhang, B. Baeumer, Tempered anomalous diffusion in heterogeneous systems. *Geophysical Research Letters* **35**, No 17 (2008); DOI: 10.1029/2008GL034899.

[31] I. Podlubny, Mittag-Leffler function. https://www.mathworks.com/matlabcentral/fileexchange/8738-mittag-leffler-function (2012).

[32] I. Podlubny, T. Skovranek, I. Petras, V. V. Verbickij, Y. Chen, B. M. V. Jara, Discrete fractional calculus: non-equidistant grids and variable step length. In: *ASME 2011 International Design Engineering Technical Conferences and Computers and Information in Engineering Conference*, American Society of Mechanical Engineers, (2011), 211–217.

[33] J. Quintana-Murillo, S. B. Yuste, A finite difference method with non-uniform timesteps for fractional diffusion and diffusion-wave equations. *The European Physical J., Special Topics* **222**, No 8 (2013), 1987–1998; DOI:10.1140/epjst/e2013-01979-7.

[34] H. Sankaranarayanan, *Grünwald-type Approximations and Boundary Conditions for One-sided Fractional Derivative Operators*. Ph.D. Thesis, University of Otago (2014).

[35] R. T. Sibatov, H.-G. Sun, Tempered fractional equations for quantum transport in mesoscopic one-dimensional systems with fractal disorder. *Fractal and Fractional* **3**, No 4 (2019), 47.

[36] J. Sun, D. Nie, W. Deng, Algorithm implementation and numerical analysis for the two-dimensional tempered fractional Laplacian. *arXiv Preprint*: arXiv:1802.02349 (Feb. 2018).

[37] M. Veillette, STBL: Alpha stable distributions for MATLAB. *MATLAB Central File Exchange*, Retrieved October 10, 2018.

[38] M. Zayernouri, M. Ainsworth, G. E. Karniadakis, Tempered fractional Sturm–Liouville eigenproblems. *SIAM J. on Scientific Computing* **37**, No 4 (2015), A1777–A1800; DOI:10.1137/140985536.

[39] Z. Zhang, W. Deng, H. Fan, Finite difference schemes for the tempered fractional Laplacian. *arXiv Preprint*: arXiv:1711.05056 (Nov. 2017).

[40] Z. Zhang, W. Deng, G. E. Karniadakis, A Riesz basis Galerkin method for the tempered fractional Laplacian. *SIAM J. on Numerical Analysis* **56**, No 5 (2018), 3010–3039.

[41] Y. Zhang, C. T. Green, E. M. LaBolle, R. M. Neupauer, H. Sun, Bounded fractional diffusion in geological media: Definition and Lagrangian approximation. *Water Resources Research* **52**, No 11 (2016), 8561–8577.

[42] Y. Zhang, M. M. Meerschaert, B. Baeumer, E. M. LaBolle, Modeling mixed retention and early arrivals in multidimensional heterogeneous media using an explicit Lagrangian scheme. *Water Resources Research* **51**, No 8 (2015), 6311–6337.

[43] Y. Zhang, H.-G. Sun, R. M. Neupauer, P. Straka, J. F. Kelly, B. Lu, C. Zheng, Identification of pollutant source for super-diffusion in aquifers and rivers with bounded domains. *Water Resources Research* **54**, No 9 (2018), 7092–7108.

[44] Y. N. Zhang, Z. Z. Sun, H. L. Liao, Finite difference methods for the time fractional diffusion equation on non-uniform meshes. *J. of Computational Physics* **265** (2014), 195–210; DOI:10.1016/j.jcp.2014.02.008.

[45] Y. Zhang, X. Yu, Xiangnan, X. Li, J. F. Kelly, H.-G. Sun, C. Zheng, Impact of absorbing and reflective boundaries on fractional derivative models: Quantification, evaluation and application. *Advances in Water Resources* **128** (2019), 129–144.

[46] V. M. Zolotarev, *One-Dimensional Stable Distributions*. Vol. 65, American Mathematical Soc., Providence (1986).

[1] *Division of Applied Mathematics, Brown University*
Providence, RI 02912, USA

e-mail: anna_lischke@brown.edu *Received: May 13, 2019*

[2] *U. S. Naval Research Laboratory*
Washington, DC 20375, USA

e-mail: james.kelly@nrl.navy.mil

[3] *Department of Statistics and Probability*

Michigan State University
East Lansing, MI 48824, USA
e-mail: mcubed@msu.edu

Please cite to this paper as published in:

Fract. Calc. Appl. Anal., Vol. **22**, No 6 (2019), pp. 1561–1595,
DOI: 10.1515/fca-2019-0081; at https://www.degruyter.com/view/j/fca.